Oncogene (2017), 1–11

www.nature.com/onc

ORIGINAL ARTICLE

Taxane-mediated radiosensitization derives from chromosomal missegregation on tripolar mitotic spindles orchestrated by AURKA and TPX2

M Orth[1,2,3,4], K Unger[2,5], U Schoetz[1,2], C Belka[1,2,3,6] and K Lauber[1,2,3]

Taxane-based radiochemotherapy is a central treatment option for various cancer entities in locally advanced stages. The therapeutic synergism of this combined modality approach due to taxane-mediated radiosensitization of cancer cells is well-known. However, the underlying molecular mechanisms remain largely elusive, and mechanism-derived predictive markers of taxane-based radiochemotherapy are currently not available. Here, we show that clinically relevant doses of Paclitaxel, the prototype taxane, stimulate a tripolar mode of mitosis leading to chromosomal missegregation and aneuploidization rather than interfering with cell cycle progression. This distinct mitotic phenotype was interlinked with Paclitaxel-mediated radiosensitization via overexpression of mitotic Aurora kinase A (AURKA) and its cofactor TPX2 whose knockdown rescued the bipolar mode of cell division and largely attenuated the radiosensitizing effects of Paclitaxel. In the cancer genome atlas (TCGA) lung adenocarcinoma cohort, high expression levels of AURKA and TPX2 were associated with specifically improved overall survival upon taxane-based radiochemotherapy, but not in case of non-taxane-based radiochemotherapy, chemo- or radiotherapy only. Thus, our data provide insights into Paclitaxel-mediated radiosensitization on a mechanistic and molecular level and identify AURKA and TPX2 as the first potential mechanism-based, predictive markers of taxane-based radiochemotherapy.

Oncogene advance online publication, 4 September 2017; doi:10.1038/onc.2017.304

INTRODUCTION

Taxane-based radiochemotherapy is of central importance for the treatment of various locally advanced cancer entities, including lung cancer.[1–4] So far, the therapeutic synergism of this regimen and taxane-mediated radiosensitization *per se* have predominantly been attributed to M-phase arrest ensuing from general stabilization of microtubules.[5–7] However, it remains controversial if clinically relevant doses of taxanes are sufficient for the induction of M-phase arrest, and the involvement of other mechanisms, including NF-κB activation and modulation of apoptotic signaling pathways, is still being discussed.[8–14] Overall, despite its unambiguous clinical relevance, the molecular basis of taxane-mediated radiosensitization remains poorly understood. Accordingly, mechanism-derived biomarkers of taxane-based radiochemotherapy are lacking, and rational patient stratification is currently not possible.

Here, we show that clinically relevant doses of Paclitaxel, the most common member of the taxane family, induce aneuploidy in various cancer cell lines as a result of multipolar mitosis and subsequent missegregation of chromosomes. The predominant mitotic phenotype was a tripolar one, and its occurrence correlated well with Paclitaxel-mediated radiosensitization. On a molecular level, we observed this effect to depend on elevated expression levels of the mitotic kinase Aurora A (AURKA) and its cofactor, the Targeting protein of XKlp2 (TPX2)—two proteins involved in assembly of the mitotic spindle and known to contribute to malignant transformation as well as therapy resistance in multiple cancer entities.[15–20] Silencing of TPX2 and AURKA expression by RNA interference (RNAi) resulted in abrogation of both tripolar spindle assembly and radiosensitization. In accordance, we observed the relative expression levels of AURKA and TPX2 to be of predictive value for the clinical outcome of taxane-based radiochemotherapy in the TCGA lung adenocarcinoma cohort. Thus, we suggest AURKA and TPX2 as potential stratification markers for taxane-based radiochemotherapy whose strength deserves further in-depth validation.

RESULTS

Low nanomolar doses of Paclitaxel stimulate the early emergence of hypodiploid cells that are not apoptotic

Recently, it has been shown that taxane-mediated M-phase arrest is dispensable for the abrogation of tumor growth and the induction of tumor cell death. The observed intratumoral concentrations of Paclitaxel in breast cancer samples were not sufficient to trigger sustained cell cycle blockade, and *in vitro*, intracellular concentrations analogous to those measured in patient tumors were already achieved by administration of low nanomolar concentrations of Paclitaxel (5–10 nM).[9] Historically however, considerably higher doses were employed to examine the mechanisms underlying taxane-mediated radiosensitization. Therefore, the present study was designed to explore the impact

[1]Department of Radiation Oncology, Ludwig-Maximilians-University of Munich, Munich, Germany; [2]Clinical Cooperation Group 'Personalized Radiotherapy in Head and Neck Cancer' Helmholtz Center Munich, German Research Center for Environmental Health GmbH, Neuherberg, Germany; [3]German Cancer Consortium (DKTK), Munich, Germany; [4]German Cancer Research Center (DKFZ), Heidelberg, Germany; [5]Research Unit of Radiation Cytogenetics, Helmholtz Center Munich, Neuherberg, Germany and [6]German Center for Lung Research (DZL), Munich, Germany. Correspondence: Dr K Lauber, Ludwig-Maximilians-University of Munich, Department of Radiation Oncology, Marchioninistr. 15, 81377 Munich, Germany.
E-mail: kirsten.lauber@med.uni-muenchen.de
Received 15 January 2017; revised 29 June 2017; accepted 20 July 2017

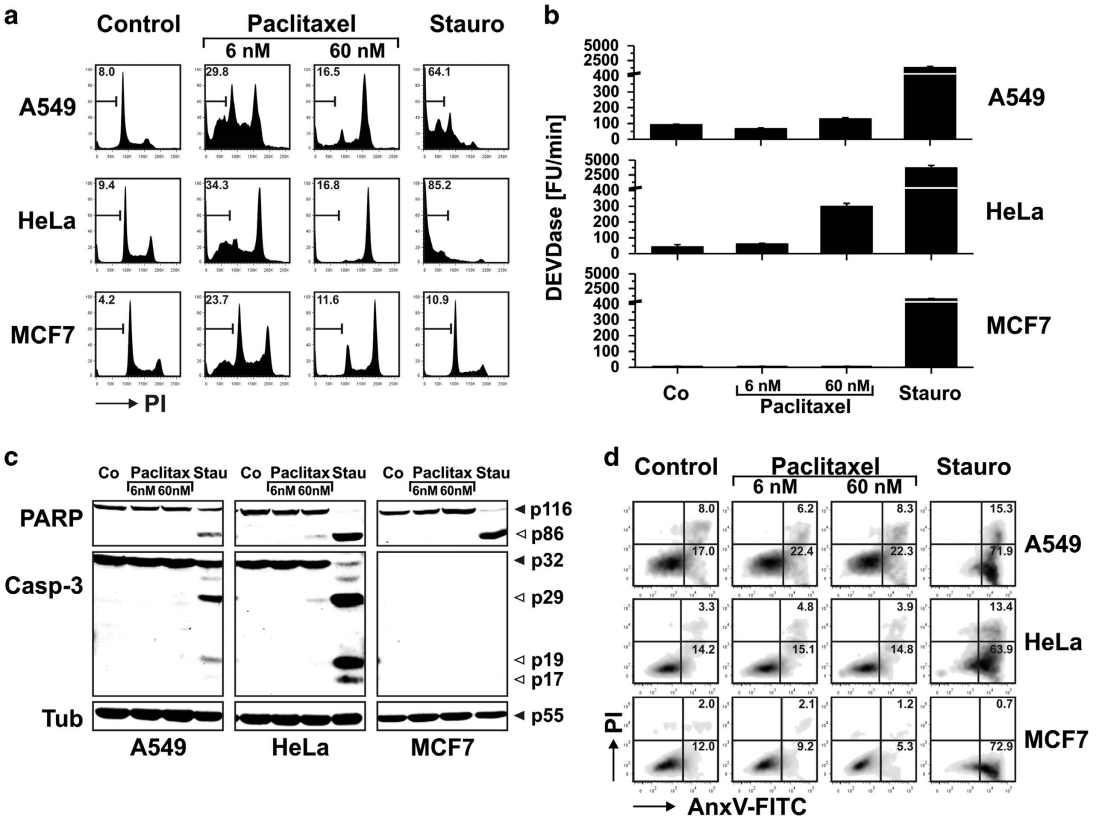

Figure 1. Low nanomolar doses of Paclitaxel stimulate the early emergence of hypodiploid cells that are not apoptotic. (**a**) Flow cytometric analysis of DNA content in A549, HeLa and MCF7 cells treated with 6 nM or 60 nM Paclitaxel for 15 h, or 5 μM Staurosporine for 5 or 15 h (positive control for apoptosis induction). The percentage of subG1 cells is depicted in representative histograms. (**b**) Measurement of DEVDase (caspase-3/-7) activity in cells treated as in (**a**). Caspase activity is shown as increase in fluorescence over time (FU/min). Means+s.d. of three replicates are displayed. (**c**) Western blot analyses of caspase-3 and PARP cleavage upon treatment as in (**a**). 200 or 20 μg of total protein were used, tubulin served as loading control. Filled arrow heads indicate the full-length forms and open arrow heads the processed forms with their respective molecular weights. (**d**) Flow cytometric analysis of phosphatidylserine exposure in A549, HeLa and MCF7 cells treated as in (**a**) for 5 h. Representative density plots are depicted, and the percentages of early and late apoptotic cells are indicated.

of low nanomolar concentrations of Paclitaxel on tumor cell radiosensitivity.

Treatment of three cancer cell lines (A549, HeLa, MCF7) with Paclitaxel doses within the lower nanomolar range stimulated the appearance of hypodiploid (subG1) cells (Figure 1a, Supplementary Figures 2A,B). Kinetically, these subG1 cells emerged as soon as 12 h after treatment, whereas exposure to higher doses of Paclitaxel required 24 h and longer for the subG1 fraction to appear. Of note, transient accumulation of G2/M-phase cells was only observed upon treatment with 60–100 nM Paclitaxel, clearly pointing towards distinct cellular reactions stimulated by these different dose ranges (Supplementary Figures 2A,B). The early-onset subG1 population was most prominent upon administration of 6 nM Paclitaxel; thus we chose this concentration for subsequent experiments.

As subG1 DNA content is a common characteristic of apoptosis, we next examined whether cells treated with low nanomolar doses of Paclitaxel for up to 15 h were in fact apoptotic. Cardinal features of apoptosis comprise caspase activation, caspase substrate cleavage and externalization of phosphatidylserine.[21] However, none of these was observed upon treatment with 6 nM Paclitaxel for up to 15 h to relevant extents and particularly not in the samples with the highest percentage of subG1 cells (Figures 1b–d). In consequence, these early-onset subG1 cells induced by low-dose Paclitaxel cannot be considered apoptotic. 60 nM of Paclitaxel were used as a control for M-phase arrest with subsequent apoptosis induction starting with caspase activation around 15 h after stimulation, and Staurosporine served as prototypical apoptosis stimulus.

Low nanomolar doses of Paclitaxel induce tripolarity of mitotic spindles, chromosomal missegregation and aneuploidy, resulting in a delayed type of apoptotic cell death

To elucidate the mechanisms by which low doses of Paclitaxel stimulate the occurrence of subG1 cells, live-cell microscopy was performed using a HeLa cell line stably expressing mCherry-histone H2B and EGFP-tubulin β.[22] After treatment with 6 nM of Paclitaxel the majority of cells displayed a tripolar type of cell division, giving rise to supernumerary daughter cells with subG1 DNA content (Supplementary Figure 1A). Similar observations were made with A549, HeLa wild-type and MCF7 cells, and quantitative analyses revealed up to 90% of multipolar (mostly tripolar) mitotic spindles (Figures 2a and b). Treatment with 6 nM of Paclitaxel resulted in the formation of ectopic microtubule-organizing centers upon mitotic entry which subsequently clustered together, thus forming the third spindle pole (Supplementary Figure 1B). The formation of this pole was independent of centrosome function as indicated by the absence of centrin (Supplementary Figure 1C). Alignment and segregation of chromosomes on these tripolar spindles occurred in a tripartite instead of a bipartite fashion (Figures 2c and d, Supplementary Figure 1A), explaining the emergence of aneuploid daughter cells with subG1 content in the FACS profile (Figure 1a). In addition, we found a substantial amount of

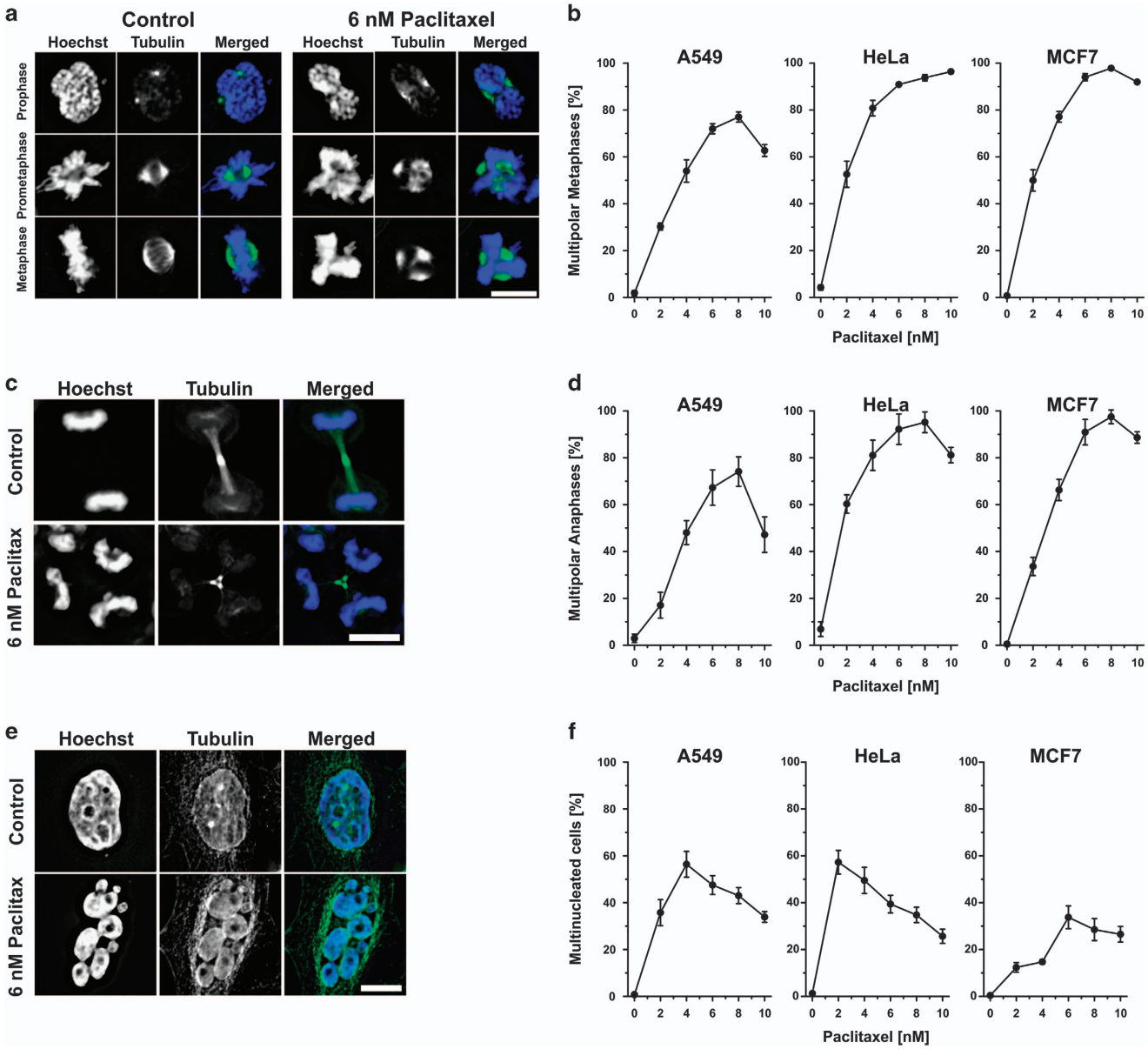

Figure 2. Low nanomolar doses of Paclitaxel induce a tripolar mitotic spindle phenotype. (**a**) Immunofluorescence microscopy of early mitotic HeLa cells treated with 6 nM Paclitaxel or DMSO/ethanol as vehicle control for 15 h and stained for tubulin (green) and DNA (blue). Scale bar depicts 10 μm. (**b**) Quantification of metaphase A549, HeLa and MCF7 cells with more than two spindle poles after treatment with indicated doses of Paclitaxel for 15 h. Means ± s.d. of four replicates are depicted. (**c**–**f**) Immunofluorescence microscopy and quantification of late anaphase (**c**,**d**) and interphase (**e**,**f**) HeLa cells treated and stained as in (**a**). Means ± s.d. of four replicates are shown, and scale bars correspond to 10 μm.

multinucleated cells (Figures 2e and f), presumably originating from unstable spindle poles dismantling during anaphase (Supplementary Figure 1D).

Whereas cellular viability was preserved upon treatment with low doses of Paclitaxel in the early stages, later on classical features of apoptosis, including caspase activation, and DNA fragmentation were observed (Supplementary Figure 2). Interestingly, the time course of caspase activation displayed clear differences between high-dose and low-dose Paclitaxel suggesting an upstream involvement of caspase-2 in the low-dose setting as already reported by others (Supplementary Figure 2D).[23,24] Hence, different dose ranges of Paclitaxel can induce apoptosis—yet via discrepant mechanisms and with different kinetics.

Radiosensitization of cells by low-dose Paclitaxel is associated with induction of the tripolar spindle phenotype

The question that arises at this point is if induction of the tripolar spindle phenotype and the resulting chromosomal missegregation are of relevance for the known radiosensitizing effects of Paclitaxel.[7,25] To this end, we analyzed clonogenic survival upon ionizing irradiation with and without low-dose Paclitaxel pre-treatment for one doubling time (Supplementary Figure 3). This approach was deliberately chosen to ensure that cells were allowed to undergo one tripolar cell division before being irradiated. Pre-treatment of all three cell lines reduced clonogenic survival to significant extents, indicating that low-dose Paclitaxel is well able to sensitize cancer cells to ionizing irradiation independently of M-phase arrest (Figure 3a). Quantitatively,

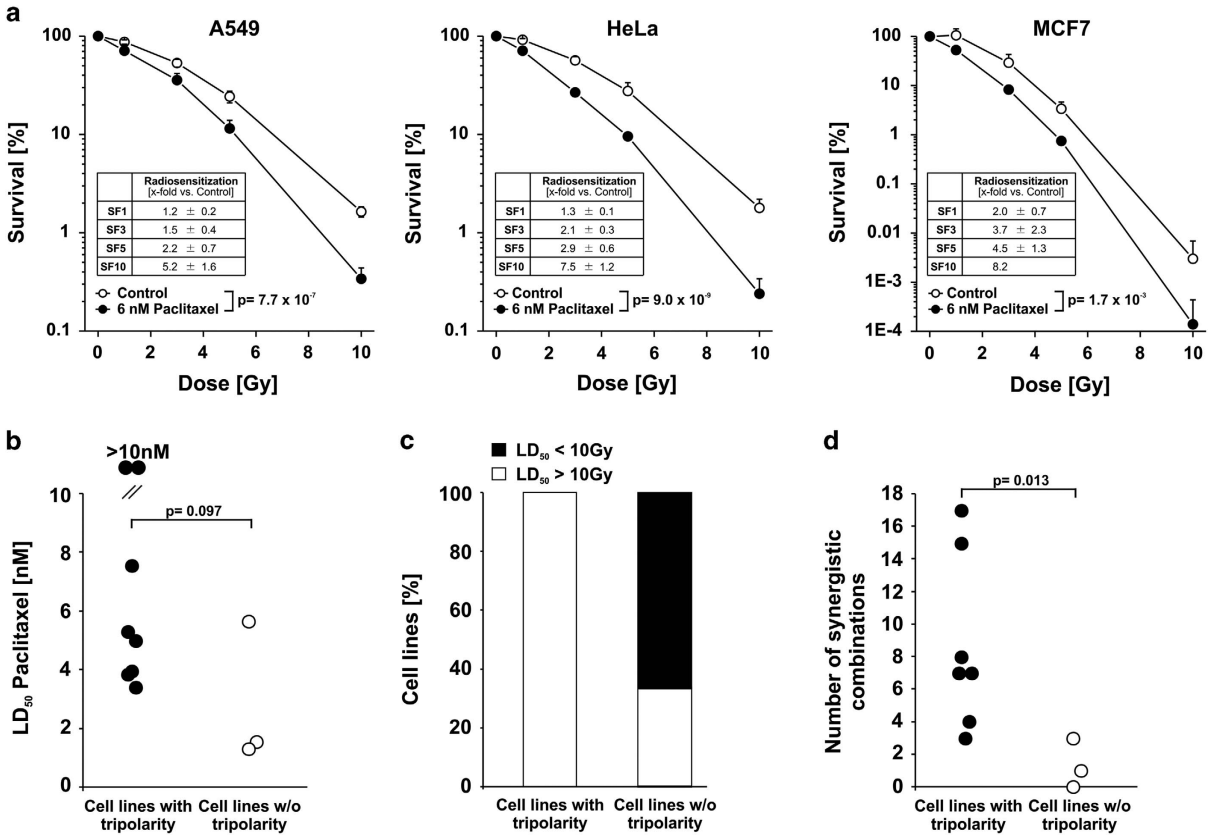

Figure 3. Occurrence of the tripolar spindle phenotype correlates with Paclitaxel-mediated radiosensitization. (**a**) Clonogenic survival assay. A549, HeLa and MCF7 cells were treated with 6 nM Paclitaxel or DMSO/ethanol for one doubling time (Supplementary Figure 3) prior to irradiation at the indicated doses. Means+s.d. of five independent replicates are shown. Overall comparison of survival curves was performed by two-way ANOVA. (**b**) LD_{50} values for Paclitaxel treatment as determined by viability tests in cell lines with spindle tripolarity and in cell lines without (Supplementary Figure 5, Supplementary Table). Cells were treated with Paclitaxel for 24 h before irradiation, and viability was assessed by Alamar blue tests after 96 h. Group comparison was performed by one-sided exact Wilcoxon Rank test. (**c**) LD_{50} values for irradiation as determined in viability tests after treatment as in (**b**). (**d**) Numbers of synergistic combinations of low-dose Paclitaxel and irradiation after treatment as in (**b**) and calculated on the basis of combination indices (Supplementary Table 2). Group comparison was performed by one-sided exact Wilcoxon Rank test.

radiosensitization reached enhancement factors of 1.2- to 8.2-fold. Not surprisingly, higher concentrations of Paclitaxel (60 nM) led to even stronger radiosensitization—most likely by engaging additional mechanisms, including spindle assembly checkpoint activation (Supplementary Figure 4). However, it needs to be emphasized that the clinical relevance of high-dose-Paclitaxel-mediated radiosensitization remains questionable, since *in vitro*, intracellular concentrations equivalent to those detected in patient tumors are already attained by administration of low nanomolar concentrations of Paclitaxel (5–10 nM).[9]

To further substantiate our findings, a panel of 11 human cancer cell lines was employed and screened for phenotypic responses towards low nanomolar doses of Paclitaxel with and without additional irradiation (Supplementary Table 1, Supplementary Figure 5). Three of the cell lines in our panel did not display detectable mitotic tripolarity after treatment with 6 nM Paclitaxel (Supplementary Table 1). When comparing the individual LD_{50} values, there was a trend towards higher resistance against the single treatments in cell lines exhibiting the tripolar phenotype (Figures 3b and c). Most importantly, a significant increase in synergism between both treatments—as calculated on the basis of combination indices—was observed (Supplementary Table 2, Figure 3d). Although the panel with 11 cell lines has its limitations, these data indicate that aneuploidization of dividing cells as a result of chromosomal missegregation appears to be involved in Paclitaxel-mediated radiosensitization.

High expression levels of AURKA and TPX2 predict tripolar spindle formation in response to low-dose Paclitaxel

On the phenotypic level, the occurrence of tripolar spindles seems to be a surrogate marker of radiosensitization by low-dose Paclitaxel. However, due to its functional nature the potential for clinical translation of this marker clearly is limited, and the underlying molecular details remain ill defined. By screening a set of crucial mitosis regulators in our cell line panel, we identified the expression levels of AURKA and its cofactor, the Targeting protein of XKlp2 (TPX2) to be the most promising predictors of Paclitaxel-induced mitotic tripolarity (Figure 4). On the mRNA level, cell lines displaying the tripolar phenotype revealed significantly higher expression levels of AURKA and TPX2 than cell lines not showing this phenotype. The same was true for a combined score of AURKA and TPX2—most likely due to the fact that their expression levels obviously are tightly coupled (Figures 4a and b). When analyzing the protein levels, the differences in individual expression values of AURKA and TPX2 did not reach statistical significance, but the difference in the combined score did (Figures 4c and d). Although expression levels and gene copy numbers mostly are not directly linked, a corresponding trend was

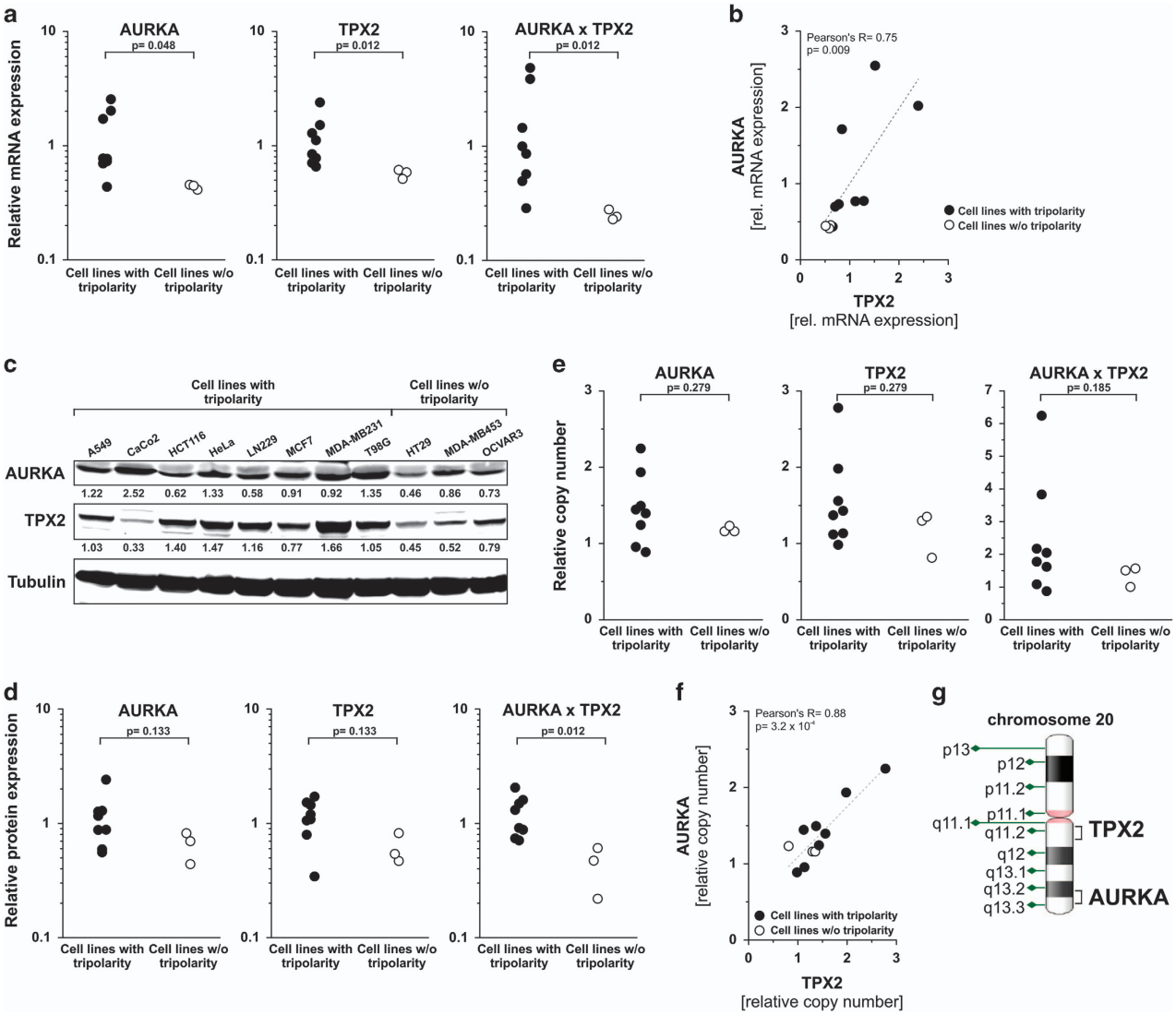

Figure 4. Tripolar mitotic spindle formation in response to low-dose Paclitaxel correlates with the expression levels of AURKA and TPX2. (**a**) qRT–PCR analyses of AURKA and TPX2 mRNA expression levels in cell lines with mitotic tripolarity and in cell lines without (Supplementary Table 1). mRNA expression was normalized on 18S rRNA and calibrated on the mean of all cell lines. The combined score was calculated as the product of AURKA and TPX2 mRNA expression. Groups were compared by two-sided exact Wilcoxon Rank test. (**b**) Pearson correlation analysis of AURKA and TPX2 mRNA expression levels obtained in (**a**). (**c**) Western blot analyses of AURKA and TPX2 protein expression levels in cell lines with spindle tripolarity and cell lines without. 200 or 20 μg of total protein were used, and tubulin served as loading control. Integrated band intensities are indicated. (**d**) Quantification of AURKA and TPX2 protein levels obtained in (**c**). Integrated band intensities were normalized on tubulin and calibrated on the mean of all cell lines. The combined score was calculated as the product of AURKA and TPX2 mRNA protein levels. Groups were compared by two-sided exact Wilcoxon Rank test. (**e**) AURKA and TPX2 relative gene copy numbers in cell lines with mitotic tripolarity and cell lines without. Relative gene copy numbers were determined by qRT–PCR, normalized using the pBiomarker multi-copy reference, and calibrated on human placenta DNA. Group comparison was performed by two-sided exact Wilcoxon Rank test. (**f**) Pearson correlation analysis of AURKA and TPX2 gene copy numbers as obtained in (**e**). (**g**) Schematic drawing of human chromosome 20 depicting gene loci of TPX2 and AURKA on 20q.

even observed on the genomic DNA level, suggesting that apart from the functional relationship of AURKA and TPX2 a genetic interconnection does exist (Figures 4e and f).[17,26] As such, both genes are located on chromosome 20q (Figure 4g).

Targeted silencing of TPX2 and AURKA protein levels restores bipolar spindle formation and abrogates Paclitaxel-mediated radiosensitization

To evaluate the causal involvement of AURKA and TPX2 in Paclitaxel-mediated radiosensitization, TPX2 expression in A549 lung adenocarcinoma cells was silenced by an RNAi approach (Figure 5). Inherently, complete depletion of TPX2 led to permanent cell cycle arrest and cell death (data not shown).[27,28] Thus, expression levels were carefully titrated to approximately 10–40% of residual protein (Figure 5a). As expected, the decrease in TPX2 levels was paralleled by a similar decrease in AURKA levels, since AURKA stability is known to depend on TPX2 (Figures 5a and b).[29] Using this setup, we observed that silencing of TPX2 and AURKA expression dose-dependently restored bipolar spindle morphology in the presence of low-dose Paclitaxel (Figures 5a and c). Quantitative analyses revealed clear-cut positive correlations between the expression levels of the two proteins and the occurrence of spindle tripolarity, and a reduction to 32% (AURKA) and 17% (TPX2) of residual protein led to a nearly complete rescue of bipolar spindle formation (Figures 5a and d). Accordingly,

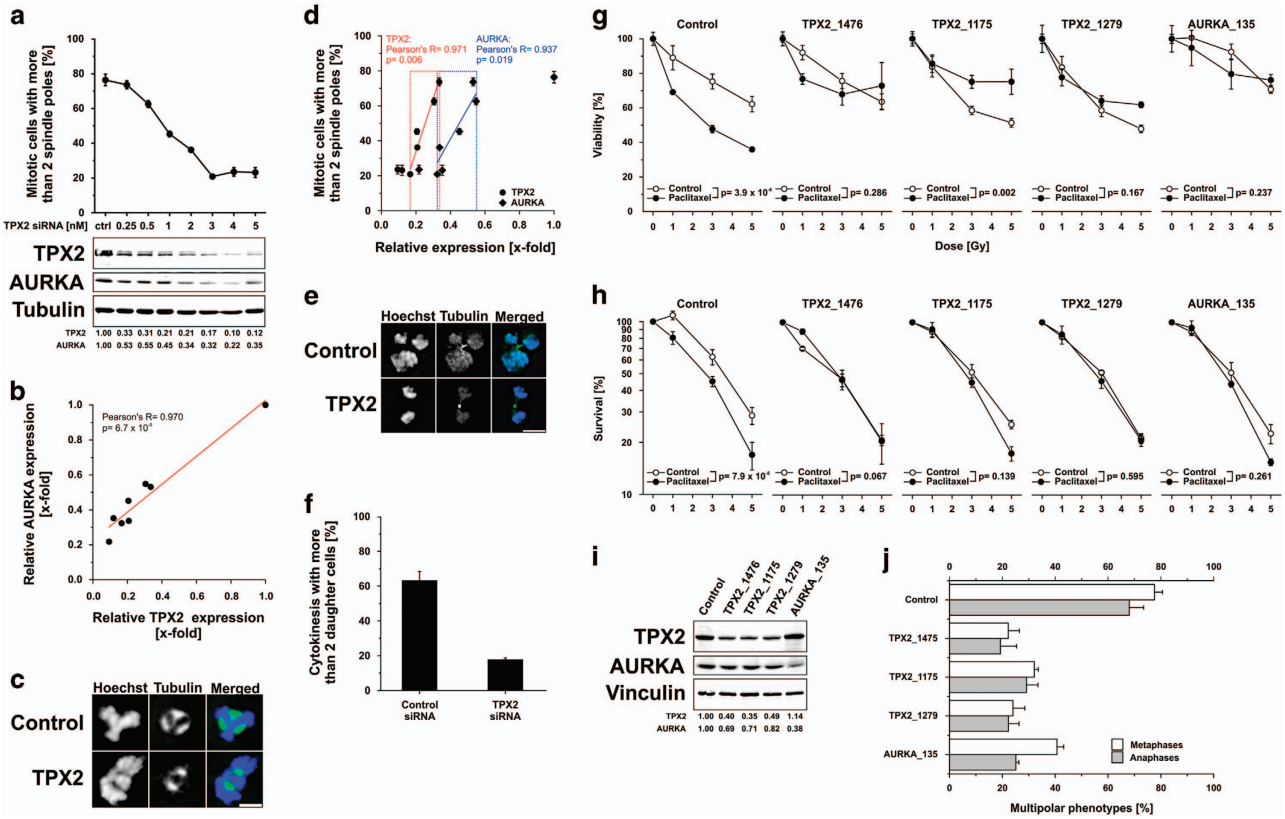

Figure 5. Decreasing TPX2 and AURKA protein expression levels restores bipolar spindle formation and abrogates radiosensitization by Paclitaxel. (**a**) Quantification of metaphase A549 cells with more than two spindle poles after transfection with the indicated concentrations of TPX2_1476 siRNA and subsequent treatment with 6 nM Paclitaxel for 24 h (upper panel). Means ± s.d. of three replicates are displayed. Western blot analyses of TPX2 and AURKA protein levels in A549 cells treated as above (lower panel). 200 or 20 μg of total protein were used and tubulin served as loading control. Relative protein expression levels were calculated by normalization of integrated band intensities on tubulin and calibration on the scramble controls. (**b**) Pearson correlation analysis of AURKA and TPX2 protein expression levels obtained in (**a**). (**c**) Immunofluorescence microscopy of early metaphase A549 cells treated with 6 nM Paclitaxel or DMSO/ethanol for 24 h after transfection with 3 nM TPX2_1476 siRNA. Cells were stained for tubulin (green) and DNA (blue). Scale bar depicts 10 μm. (**d**) Pearson correlation analysis of the percentage of metaphase cells with more than two spindle poles and protein expression levels of TPX2 and/or AURKA after treatment as in (**a**). (**e**) Immunofluorescence microscopy of late anaphase A549 cells treated and stained as in (**c**). (**f**) Quantification of anaphase A549 cells yielding more than two daughter cells after treatment as in (**c**). Means+s.d. of three replicates are shown. (**g**) Viability of A549 cells transfected with 3 nM control, TPX2 or AURKA siRNA, treated with 6 nM Paclitaxel for one doubling time, and irradiated at the indicated doses. Viability was assessed 120 h after irradiation by Alamar blue tests. Comparison of the curves was performed by two-way ANOVA. (**h**) Clonogenic survival of A549 cells treated as in (**g**). Comparison was performed by two-way ANOVA. (**i**) Western blot analyses of TPX2 and AURKA protein levels in A549 cells treated as in (**g**) and quantified as in (**a**). (**j**) Quantification of meta- and anaphase A549 cells with more than two spindle poles after transfection with the indicated siRNA oligonucleotides and subsequent treatment with 6 nM Paclitaxel for 24 h. Means ± s.d. of three replicates are shown.

adequate bipartite cytokinesis was also restored (Figures 5e and f), implying that TPX2 and AURKA are a prerequisite for the induction of tripolar mitosis and resulting aneuploidy by low-dose Paclitaxel. Since our study identified the association of mitotic tripolarity and Paclitaxel-mediated radiosensitization, we next determined the influence of TPX2 RNAi in this scenario (Figures 5g and h). In order to exclude off-target effects of the siRNA oligonucleotide that had been used so far (TPX2_1476), we included two more TPX2-targeting siRNA oligonucleotides (TPX2_1175 and TPX2_1279) and one AURKA-specific siRNA oligonucleotide (AURKA_135) into these analyses. Not surprisingly, the various siRNA oligonucleotides differed slightly in terms of their knockdown efficiency (Figure 5i). Yet, in all cases bipolar mitosis upon Paclitaxel-treatment was restored and corresponding radiosensitization was almost completely abrogated both in viability as well as in clonogenic survival assays (Figures 5g,h,j). It needs to be noted that in case of AURKA, siRNA-mediated silencing rescued bipolar mitosis only in part. The appearance of taxane-induced mitotic tripolarity was significantly reduced, but instead we observed other aberrant mitotic phenotypes with single or highly fragmented spindle poles which most likely originate from AURKA's multiple functions in centrosome separation, duplication and maturation apart from bipolar spindle assembly and stabilization (Supplementary Figure 6).[30]

These findings finally strengthen the conclusion that TPX2 and AURKA are crucially involved in Paclitaxel-dependent radiosensitization and might serve as stratification markers in Paclitaxel-based radiochemotherapy approaches.

High expression levels of AURKA and TPX2 are associated with improved clinical outcome of taxane-based radiochemotherapy in the TCGA lung adenocarcinoma cohort

As a first approach to assess the predictive value of AURKA and TPX2 in the context of taxane-based radiochemotherapy, we took advantage of TCGA lung adenocarcinoma cohort representing 114 patients in total with 13 patients undergoing taxane-based and 19 patients undergoing non-taxane-based concomitant radiochemotherapy (Figure 6a). As already indicated in our *in vitro* studies, the mRNA expression levels of TPX2 and AURKA were closely

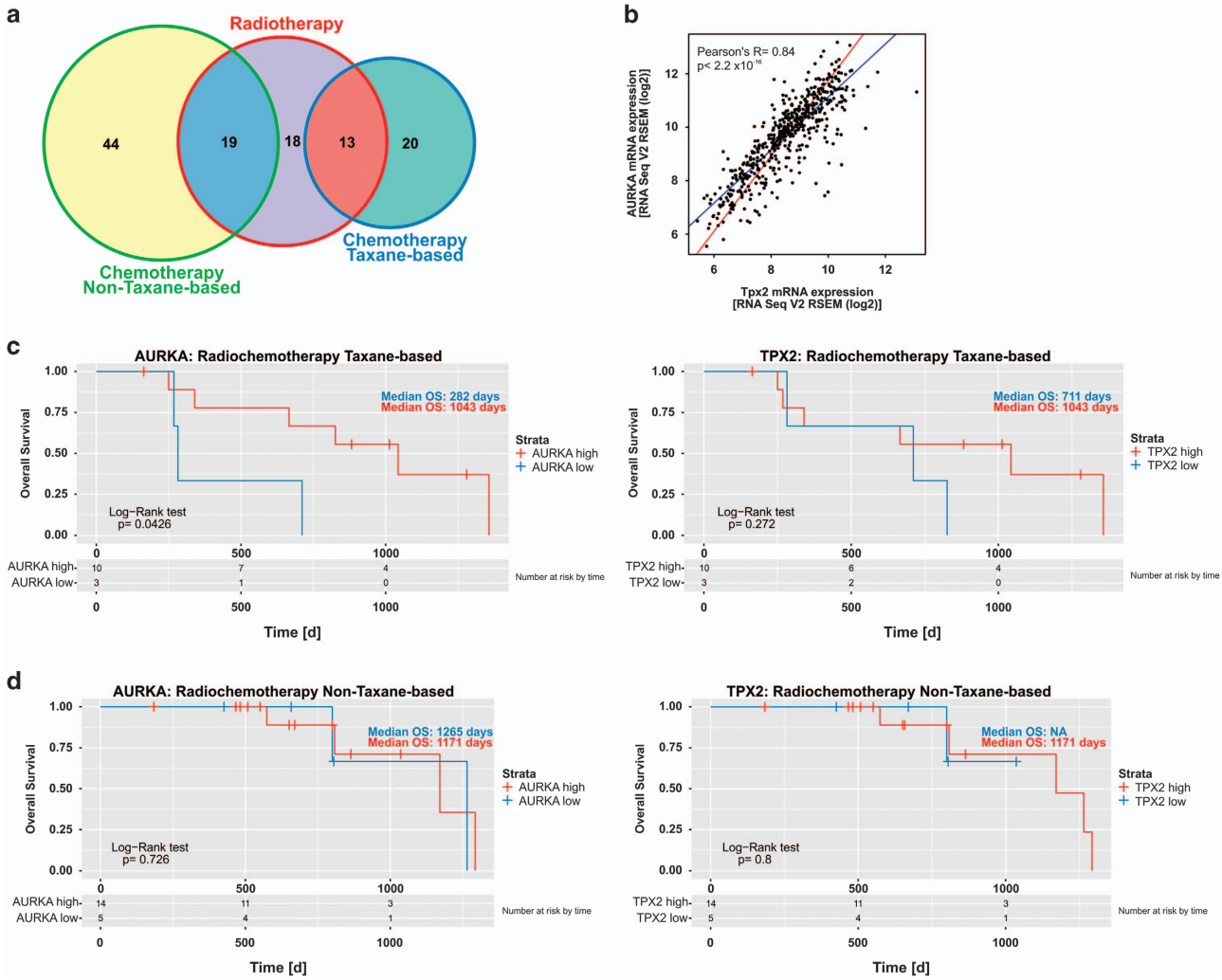

Figure 6. High expression levels of AURKA and TPX2 are associated with improved clinical outcome of taxane-based radiochemotherapy. (**a**) TCGA lung adenocarcinoma patient cohort divided by their respective treatment regimens. (**b**) Pearson correlation of AURKA and TPX2 mRNA expression levels in the TCGA cohort. (**c**) Kaplan–Meier overall survival analysis of patients undergoing taxane-based radiochemotherapy with and without overexpression of AURKA or TPX2, respectively (cut-off first quartile). (**d**) Kaplan–Meier overall survival analysis of patients undergoing non-taxane-based radiochemotherapy with and without overexpression of AURKA or TPX2, respectively (cut-off first Quartile). Comparison was performed by Log-Rank test.

correlated in the patient samples (Figure 6b). Overall survival data showed a significant therapeutic benefit for taxane-based radiochemotherapy in patients with AURKA overexpression, and a similar trend was detected for TPX2 overexpression (Figures 6c and d). In contrast, no such differences were observed for non-taxane-based radiochemotherapy, radiotherapy alone or chemotherapy alone, respectively (Supplementary Figure 7). According to our *in vitro* data, DNA copy number gains of TPX2 or AURKA were less stringently connected to improved overall survival upon taxane-based radiochemotherapy. Nevertheless, the observed tendency still reflects the assumed role of both genes in the context of Paclitaxel-mediated radiosensitization (Supplementary Figure 8).

DISCUSSION

For lung cancer and different other entities in locally advanced stages, taxanes, such as the prototypical family member Paclitaxel, represent a crucial treatment option—in chemotherapy only regimens as well as in multimodal concepts together with radiotherapy.[1,3,4] Being potent stabilizers of microtubules, their cytostatic and radiosensitizing properties so far have been largely ascribed to an interference with cell cycle progression in proliferating cells during mitosis.[5,6] In terms of radiosensitization this notion appears particularly plausible, since cultured mammalian cells are known to be most vulnerable towards irradiation during M-phase in which several DNA damage repair mechanisms are actively shut off.[31–33] However, this model has recently been questioned, and it was suggested that the cytotoxic effects of Paclitaxel instead derive from a missegregation of chromosomes on multipolar spindles.[9,10] Importantly, the authors showed that low nanomolar concentrations of Paclitaxel, when applied to cultured cancer cells *in vitro*, result in intracellular concentrations similar to those measured after systemic administration in breast cancer samples where multipolar mitotic spindles were observed.[9] This stimulated us to examine whether chromosomal missegregation also accounts for taxane-mediated radiosensitization rather than the M-phase arrest that historically has been proposed by various *in vitro* studies in which considerably higher concentrations of Paclitaxel were employed.[7] Our data provide evidence that low-dose Paclitaxel which is sufficient to stimulate mitotic tripolarity but fails to induce M-phase arrest can potently sensitize cancer cells to ionizing irradiation. Intriguingly, induction of the tripolar mitotic phenotype and radiosensitization were closely

coupled, and the therapeutic synergism between low-dose Paclitaxel and irradiation was preferentially pronounced in cancer cells which exhibit Paclitaxel-induced mitotic tripolarity.

Molecularly, we identified the mitotic AURKA and its cofactor TPX2 to be essentially involved in this scenario. Both are known to be frequently overexpressed in cancer, to participate in oncogenic transformation, and to contribute to therapy resistance.[15,16,18–20,34,35] Although our screening panel of 11 cell lines has its limitations, we observed that cell lines displaying the tripolar mitotic phenotype express higher levels of AURKA and TPX2 on the protein and the mRNA level—in part due to genomic amplification of the respective gene loci. These high expressers were considerably more resistant towards low-dose Paclitaxel and irradiation in the monotreatment settings, thus underlining the contribution of AURKA and TPX2 to therapy resistance.[35–38] However, the therapeutic synergism between the two regimens was clearly increased, and it was abrogated upon downregulation of TPX2 and Aurora A expression. This allows the conclusion that mitotic tripolarity and radiosensitization by low-dose Paclitaxel are interlinked via high expression levels of AURKA and TPX2. Mechanistically, both proteins act in concert by forming a dimeric complex which results in allosteric activation of AURKA as well as its proper recruitment to mitotic spindles.[39–41] The TPX2/AURKA complex is involved in nucleation and stabilization of microtubules, although the molecular details remain largely elusive.[42] It is considered to be of pivotal importance for the formation of centrosome-independent microtubule-organizing centers during mitosis, thus strongly supporting the notion that it is also required for Paclitaxel-stimulated assembly of supernumerary spindle poles.[43]

In accordance with other reports, we observed that knockdown of TPX2 coincides with a decline in AURKA levels.[29] Hence, a decrease in AURKA activity supposedly also is involved in restoration of bipolar spindle formation—an assumption which is further strengthened by our AURKA-targeting siRNA approach. However, several studies showed that pharmacologic inhibition of AURKA synergizes with Paclitaxel treatment in terms of abrogation of cell proliferation and induction of cell death.[44–47] Appearing as a contradiction to our results at first sight, it needs to be considered that AURKA inhibitors interfere with total AURKA activity irrespective of its subcellular localization. In contrast, we selectively reduced the expression levels of TPX2 and the amount of available TPX2/AURKA complex. This decrease resulted in restoration of mitotic bipolarity and abrogation of Paclitaxel-mediated radiosensitization. On the contrary, complete AURKA inhibition by the highly AURKA-specific compound Alisertib[48] led to a striking increase in aberrant mitotic phenotypes, including disturbed mitotic entry, monopolar spindle formation, erroneous centrosome separation and cytokinesis failure (data not shown), thus rendering detailed analyses of Alisertib's impact on Paclitaxel-mediated mitotic tripolarity and radiosensitization completely impossible. We suggest that the synergism reported for AURKA inhibitors and other drugs needs to be attributed to these distinct aberrant mitotic phenotypes.[49] In contrast, for Paclitaxel-stimulated formation of additional spindle poles and corresponding radiosensitization, we propose that only the TPX2-complexed pool of AURKA is involved, whereas other subcellular AURKA pools localized to the chromatin or the centrosomes, respectively, are not.

Using the TCGA lung adenocarcinoma cohort, we could show that high expression levels of AURKA and TPX2 are associated with improved overall survival in response to taxane-based radiochemotherapy, but not in case of non-taxane-based radiochemotherapy, chemo- or radiotherapy only. These findings render AURKA and TPX2 the first potential mechanism-derived predictive markers in this context. Clearly, our data require evaluation with larger patient cohorts in prospective settings and more detailed clinical follow-up data, and it needs to be clarified which molecular level (genomic DNA, mRNA or protein expression) has the strongest predictive power. But in principle, AURKA and TPX2 seem to have the capacity to identify patients who can benefit most from taxane-based radiochemotherapy. Accordingly, rational patient stratification in the future could focus on these predicted responders and could spare designated non-responders from unnecessary side effects.

MATERIALS AND METHODS

Cells and reagents

Cell lines were purchased from ATCC (Manassas, VA, USA), DSMZ (Braunschweig, Germany) or Cell Lines Services (Heidelberg, Germany), respectively, and identity was confirmed by STR-typing (DSMZ). Cells were cultured at 37 °C and 5.0/7.5% CO_2 in respective cell culture media supplemented with 10% heat-inactivated fetal calf serum (Life Technologies, Karlsruhe, Germany), 100 U/ml penicillin, and 0.1 mg/ml streptomycin (Lonza, Cologne, Germany).

Paclitaxel and all reagents were obtained from Sigma-Aldrich (Taufkirchen, Germany) if not stated otherwise.

The following western blot antibodies were used: Rabbit anti-Aurora A/AIK, rabbit anti-cleaved caspase-3 (Cell Signaling, Leiden, the Netherlands), mouse anti-PARP (Trevigen Biozol, Eching, Germany), mouse anti-caspase-2 (Enzo Life Sciences, Lausen, Switzerland), mouse anti-caspase-3 (BD Transduction Laboratories, Heidelberg, Germany), mouse anti-Cyclin B1 (Merck Millipore, Darmstadt, Germany), mouse anti-tubulin-α, mouse anti-Vinculin (both from Sigma-Aldrich), and rabbit anti-TPX2 (gift from O.J. Gruss, Bonn, Germany).

For fluorescence microscopy, FITC- or Cy3-labeled mouse anti-tubulin-β antibody (Sigma-Aldrich) and rabbit anti-centrin antibody (gift from O. Stemmann, Bayreuth, Germany) were used.

X-ray treatment

Cells were irradiated using a Mueller RT-250 (Philips, Amsterdam, the Netherlands) or an RS-225 (X-Strahl, Camberley, UK) γ-ray tube (200 kV /10 mA, Thoraeus filter, 1 Gy in 112 or 63 s, respectively).

Clonogenic survival assays

Clonogenic survival was determined by colony formation assays as described.[50] Briefly, cells were seeded into six-well plates at ranges yielding 20–150 colonies per well. After adherence for 4 h, medium was replaced by fresh medium containing DMSO/ethanol (as control) or Paclitaxel at the indicated concentrations, and cells were incubated for one doubling time (see Supplementary Figure 3). Subsequently, medium was replaced by drug-free medium, cells were irradiated and colony formation was allowed for 14 days. Staining was performed with methylene blue (0.3% in 80% ethanol), and colonies with more than 50 cells were counted. The percentage of surviving cells was calculated and normalized on the plating efficiency.

Fluorescence microscopy and life-cell imaging

For fluorescence microscopy, cells were seeded onto coverslips in 24-well plates and treated as indicated. Cells were fixed and stained with antibodies for at least 1 h at room temperature as described.[51] DNA was visualized with Hoechst 33342 (2 μg/ml), and coverslips were mounted onto glass slides (Thermo Scientific, Schwerte, Germany). An inverse epifluorescence microscope (Zeiss AxioObserver Z1) equipped with an AxioCam Mr3 camera, a Zeiss Plan-Neofluar 63X/1.3 glycerol objective, the AxioVision 4.8 software package, and the following filters was used (all from Carl Zeiss, Jena, Germany): BP365/12 for Hoechst 33342, BP470/40 for FITC and BP550/25 for Cy3. Twenty-five z-stacks with 250 nm distance were recorded and deconvolved using the AxioVision 4.8 software (applied mode: Iterative). For life-cell imaging, HeLa cells stably expressing EGFP-tubulin β and mCherry-histone H2B[22] were seeded into eight-chamber Ibidi slides (Ibidi, Martinsried, Germany) and treated as indicated. Imaging was started after 2 h, and movies were captured for 16–24 h.

Flow cytometric analyses of cellular DNA content and phosphatidylserine externalization

Flow cytometric analyses were performed using an LSRII cytometer (BD Biosciences, Heidelberg, Germany) and FACS Diva (BD Biosciences) or Flowjo 7.6.5 software (Tree Star, Ashland, OR, USA), respectively. For DNA staining, cells were collected by trypsinization, fixed in ice-cold ethanol (70%), washed twice with phosphate-buffered saline containing 0.1% bovine serum albumin, and stained with 69 μM propidium iodide in 38 mM sodium citrate supplemented with 0.1 mg/ml RNAse A for 15 min. After doublet exclusion cellular DNA content was analyzed on the basis of propidium iodide fluorescence intensity. Externalized phosphatidylserine was detected by Annexin V-FITC/propidium iodide staining (BD Biosciences). Annexin V-FITC-positive/propidium iodide-negative cells were considered early apoptotic, and double-positive cells were considered late apoptotic/secondary necrotic.

Sodium dodecyl sulfate–polyacrylamide gel electrophoresis and western blot analyses

Reducing 6–15% gradient sodium dodecyl sulfate–polyacrylamide gel electrophoresis and western blot analyses were performed as described.[51] Briefly, whole cell lysates were prepared in lysis buffer (50 mM Tris-HCl pH 7.6, 150 mM NaCl, 1% Triton X-100, 3 μg/ml aprotinin, 3 μg/ml leupeptin, 3 μg/ml pepstatin and 2 mM phenylmethylsulfonyl fluoride), protein concentrations were determined by Bradford assay (Bio-Rad, Munich, Germany), and 20–300 μg of total protein extracts were subjected to electrophoretic separation. Proteins were transferred to Polyvinylidenfluoride Immobilon FL membranes (Merck Millipore), membranes were blocked with 5% low-fat milk powder in TBST (tris-buffered saline, supplemented with 0.02% Tween-20) buffer (13 mM Tris-HCl pH 7.5, 150 mM NaCl and 0.02% Triton X-100), and incubated with primary antibodies overnight. IRDye-conjugated secondary antibodies (LI-COR Biotechnology, Bad Homburg, Germany) were added for 1 h, membranes were extensively washed in TBST buffer, and IRDye fluorescence was recorded using a LI-COR Odyssey scanner (LI-COR Biotechnology). For relative quantification, integrated band intensities were determined, normalized onto the corresponding loading controls and calibrated as indicated.

Caspase activity assays

Caspase activity was assessed in enzymatic assays as described before.[52] Lysates were prepared as described for western blotting, and 30 μg of total protein extracts were incubated at 37 °C with 50 μM Ac-DEVD-AMC (for caspase-3/-7) for 1 h or 50 μM Ac-VDVAD-AFC (for caspase-2) for 4 h (both from Bachem, Bubendorf, Switzerland). AMC/AFC-release was measured using a microplate fluorescence reader (Synergy MX, BioTek, Bad Friedrichshall, Germany) at 360/9 nm excitation and 460/9 nm emission. Relative caspase activities were calculated from the slopes of the regression lines.

Viability assays

Cellular viability was assessed by Alamar Blue reduction assays (Bio-Rad). In brief, cells were seeded into 96-well plates and treated as indicated. After incubation for 96-120 h, medium was removed, fresh medium supplemented with 1/10 volume of Alamar Blue reagent was added, and resazurin reduction was allowed for 2–6 h at 37 °C. Resorufin fluorescence was measured using a Synergy MX microplate reader (BioTek) at 560/9 nm excitation and 590/9 nm emission. For each treatment pair a specific combination index was determined which classifies the quality of interaction between the analyzed treatment components, indicating additivity (combination index = 1), synergism (combination index < 1) or antagonism (combination index > 1), respectively.[53]

Real-time PCR for quantification of mRNA expression levels and gDNA copy numbers (qRT–PCR)

Quantification of mRNA levels by quantitative real-time (qRT)–PCR was performed as described previously.[54] Total RNA was extracted using the NucleoSpin RNA II Kit (Macherey & Nagel, Düren, Germany), and 1 μg RNA was reversely transcribed with 200 units RevertAid reverse transcriptase in the presence of 1 ng/μl random hexamers, 2.5 ng/μl Oligo$(dT)_{18}$, 50 μM dNTPs and 0.1 units/μl RiboLock RNase inhibitor (Thermo Scientific, Dreieich, Germany). qRT–PCR was performed on an LC480 qPCR platform (Roche Applied Science, Penzberg, Germany) with 20 ng cDNA per reaction and 300 nM primers (Sigma-Aldrich) in 1 × Maxima SYBR Green qPCR Mastermix (Thermo Scientific). The following primer pairs were used: hTPX2 forward 5'-TTTGGAAGATGTTGTGGGTGTTC-3', hTPX2 reverse 5'-TTCAATGCAAAGGCTGGTGAC-3', hAURKA forward 5'-TTCAGGACCTGTTAAGGCTACAGC-3', hAURKA reverse 5'-GAGCCTGGCCACTATTTACAGGT-3', 18S rRNA forward 5'-CGGCTACCACATCCAAGGAA-3' and 18S rRNA reverse 5'-GCTGGAATTACCGCGGCT-3'. For quantification, the standard curve method was employed, results were normalized on 18S rRNA as reference gene, and calibrated as indicated.

Measurement of DNA copy numbers was performed with gDNA extracted with the NucleoSpin Tissue Kit (Macherey & Nagel) in 1 × SYBR Green qPCR Mastermix with 300 nM of primers in a total volume of 20 μl. The following primer pairs were used: hTPX2 forward 5'-GTGTTCCTGAAAAGAAGGTACTT-3', hAURKA forward 5'-TGGAGGTCCAAAACGTGTTCTC-3', reverse primers as above. Relative quantification of DNA copy numbers was performed using the standard curve method employing human placenta gDNA as standard and as normal tissue control (Promega, Mannheim, Germany), and the pBiomarker copy number PCR assay multi reference kit (Qiagen, Hilden, Germany) for normalization. Pseudoreplicates of 40 ng, 8 ng and 1.6 ng gDNA per reaction were employed in order to correct for individual differences in PCR efficiencies.

Transfection of stealth siRNAs

Stealth siRNA oligonucleotides were obtained from Life Technologies. The following oligonucleotides were used: hTPX2_1476 5′-GAACAGAAUUCGAAUGCCCACCAAA-3′, hTPX2_1175 5′-AGGAGCUCGAGAAAUUGCAACAAUA-3′, hTPX2_1279 5′- CCCACCGAGCCUAUUGGCUUUGAUU-3′, hAURKA_135 5′- GCGGGUCUUGUGUCCUUCAAAUUCU-3′ and scrambled control 5′-GAAAGUACUAGUACTCCCACACAAA-3′. Transfection of siRNAs was performed using Lipofectamine 2000 (Life Technologies). Cells were seeded into 24-well plates supplemented with coverslips (for microscopy) or into 75 cm^2 cell culture flasks (for colony formation assays), respectively. Upon adherence, medium was removed, and Opti-MEM (Life Technologies) was added. Cells were transfected with the indicated siRNA concentrations for 24 h, treated with Paclitaxel for one doubling time, and subjected to the respective assays as described above.

TCGA analysis

The results are based upon data generated by the TCGA Research Network: http://cancergenome.nih.gov/. Normalized IlluminaHiSeq level 3 read counts (version 10/23/2014) generated with the TCGA RNAseq Version 2 (https://wiki.nci.nih.gov/display/TCGA/RNASeq+Version+2) of the TCGA lung adenoma data set (LUAD) along with available clinical data tables (version 12/09/2014) were downloaded from the TCGA data portal. Only data from primary tumors (sample barcode '01A') were used in the analyses. For genomic copy number analysis, the appropriate GISTIC 2.0 called level 3 data (version 04/02/2015) were downloaded using the firehose command-line tool (https://confluence.broadinstitute.org/display/GDAC/Download). Gene level copy number calls differentiated five levels, that is, complete loss [−2], single loss [−1], normal copy number [0], simple gain [1] and high-level amplification [2]. The following columns of the appropriate clinical data tables were used: bcr_patient_barcode (key column), pharmaceutical_therapy_drug_name, pharmaceutical_therapy_type, pharmaceutical_tx_started_days_to, pharmaceutical_tx_ended_days_to, radiation_therapy_started_days_to, radiation_therapy_ended_days_to, vital_status, last_contact_days_to, death_days_to. All analyses of the TCGA RNAseq and genomic copy number data were carried out using the R statistical analysis platform. The Venn diagram (Figure 6a) was generated using the R-Forge package Vennerable. Correlation between AURKA and TPX2 mRNA expression (Figure 6b) was determined using Pearson correlation, and linear models were plotted in order to visualize strength of correlation. The inner angle between the two lines reflects the correlation coefficient (0° equals $R^2 = 1$ and 90° equals $R^2 = 0$). For survival analysis, 5 years of follow-up were considered, and calculations were carried out using functions from the R survival package to build cox-proportional hazard models. Survival differences between groups were determined using Log-Rank test. Kaplan–Meier plots were generated using the ggplot-based package survMisc (Figures 6c and d, Supplementary Figures 7). As a threshold for high- and low expressers the first quartile of the distribution of the log2-transformed expression values was used. With regard to copy number analyses, GISTIC 2.0 copy number calls greater than 0 were considered to represent copy number gains and were used to dichotomize the analyzed groups into TPX2 gain/no gain and AURKA gain/no gain.

Statistical analyses

If not stated otherwise, results of *in vitro* experiments are shown as means ± s.d. of at least three independent experiments. Statistical analyses were executed with Origin 9.1 Pro software (OriginLab Corporation, Northampton, MA, USA). *P*-values were calculated by one-sided or two-sided exact Wilcoxon Rank tests, or two-way ANOVA as indicated, and correlation analyses were performed according to Pearson. The threshold for statistical significance was set as $P < 0.05$.

CONFLICT OF INTEREST

The authors declare no conflict of interest.

ACKNOWLEDGEMENTS

We thank Olaf Stemmann for the stably transfected HeLa cell line and the centrin antibody, and Oliver J. Gruss for TPX2 antisera. This work was supported by grants of the Friedrich-Baur-Stiftung and the Verein zur Förderung von Wissenschaft und Forschung to MO and CB.

AUTHOR CONTRIBUTIONS

Conception and design: M. Orth, K. Lauber; Development of methodology: M. Orth, K. Unger, K. Lauber; Acquisition of data: M. Orth, K. Unger, U. Schoetz, K. Lauber; Analysis and interpretation of data: M. Orth, K. Unger, U. Schoetz, K. Lauber; Writing and revision of manuscript: M. Orth, K. Unger, U. Schoetz, C. Belka, K. Lauber.

REFERENCES

1 Huber RM, Flentje M, Schmidt M, Pollinger B, Gosse H, Willner J *et al.* Simultaneous chemoradiotherapy compared with radiotherapy alone after induction chemotherapy in inoperable stage IIIA or IIIB non-small-cell lung cancer: study CTRT99/97 by the Bronchial Carcinoma Therapy Group. *J clin oncol* 2006; **24**: 4397–4404.
2 Janssen A, Medema RH. Mitosis as an anti-cancer target. *Oncogene* 2011; **30**: 2799–2809.
3 Eberhardt WE, Pottgen C, Gauler TC, Friedel G, Veit S, Heinrich V *et al.* Phase III study of surgery versus definitive concurrent chemoradiotherapy boost in patients with resectable stage IIIA(N2) and selected IIIB non-small-cell lung cancer after induction chemotherapy and concurrent chemoradiotherapy (ESPATUE). *J clin oncol* 2015; **33**: 4194–4201.
4 Choy H, Pyo H, Kim JS, MacRae R. Role of taxanes in the combined modality treatment of patients with locally advanced non-small cell lung cancer. *Expert Opin Pharmacother* 2001; **2**: 963–974.
5 Horwitz SB, Lothstein L, Manfredi JJ, Mellado W, Parness J, Roy SN *et al.* Taxol: mechanisms of action and resistance. *Ann NY Acad Sci* 1986; **466**: 733–744.
6 Liebmann J, Cook JA, Fisher J, Teague D, Mitchell JB. In vitro studies of Taxol as a radiation sensitizer in human tumor cells. *J Natl Cancer Inst* 1994; **86**: 441–446.
7 Pawlik TM, Keyomarsi K. Role of cell cycle in mediating sensitivity to radiotherapy. *Int J Radiat Oncol Biol Phys* 2004; **59**: 928–942.
8 Bhalla KN. Microtubule-targeted anticancer agents and apoptosis. *Oncogene* 2003; **22**: 9075–9086.
9 Zasadil LM, Andersen KA, Yeum D, Rocque GB, Wilke LG, Tevaarwerk AJ *et al.* Cytotoxicity of paclitaxel in breast cancer is due to chromosome missegregation on multipolar spindles. *Sci Transl Med* 2014; **6**: 229ra243.
10 Demidenko ZN, Kalurupalle S, Hanko C, Lim CU, Broude E, Blagosklonny MV. Mechanism of G1-like arrest by low concentrations of paclitaxel: next cell cycle p53-dependent arrest with sub G1 DNA content mediated by prolonged mitosis. *Oncogene* 2008; **27**: 4402–4410.
11 Dey S, Spring PM, Arnold S, Valentino J, Chendil D, Regine WF *et al.* Low-dose fractionated radiation potentiates the effects of Paclitaxel in wild-type and mutant p53 head and neck tumor cell lines. *Clin cancer res* 2003; **9**: 1557–1565.
12 Giannakakou P, Robey R, Fojo T, Blagosklonny MV. Low concentrations of paclitaxel induce cell type-dependent p53, p21 and G1/G2 arrest instead of mitotic arrest: molecular determinants of paclitaxel-induced cytotoxicity. *Oncogene* 2001; **20**: 3806–3813.
13 Steren A, Sevin BU, Perras J, Ramos R, Angioli R, Nguyen H *et al.* Taxol as a radiation sensitizer: a flow cytometric study. *Gynecol Oncol* 1993; **50**: 89–93.
14 Kurdoglu B, Cheong N, Guan J, Corn BW, Curran WJ Jr, Iliakis G. Apoptosis as a predictor of paclitaxel-induced radiosensitization in human tumor cell lines. *Clin cancer res* 1999; **5**: 2580–2587.
15 Wang H, Liang L, Fang JY, Xu J. Somatic gene copy number alterations in colorectal cancer: new quest for cancer drivers and biomarkers. *Oncogene* 2016; **35**: 2011–2019.
16 Goldenson B, Crispino JD. The aurora kinases in cell cycle and leukemia. *Oncogene* 2015; **34**: 537–545.
17 Neumayer G, Belzil C, Gruss OJ, Nguyen MD. TPX2: of spindle assembly, DNA damage response, and cancer. *Cell Mol Life Sci* 2014; **71**: 3027–3047.
18 Sillars-Hardebol AH, Carvalho B, Tijssen M, Belien JA, de Wit M, Delis-van Diemen PM *et al.* TPX2 and AURKA promote 20q amplicon-driven colorectal adenoma to carcinoma progression. *Gut* 2012; **61**: 1568–1575.
19 Yang G, Chang B, Yang F, Guo X, Cai KQ, Xiao XS *et al.* Aurora kinase A promotes ovarian tumorigenesis through dysregulation of the cell cycle and suppression of BRCA2. *Clin cancer res* 2010; **16**: 3171–3181.
20 Warner SL, Stephens BJ, Nwokenkwo S, Hostetter G, Sugeng A, Hidalgo M *et al.* Validation of TPX2 as a potential therapeutic target in pancreatic cancer cells. *Clin cancer res* 2009; **15**: 6519–6528.
21 Galluzzi L, Bravo-San Pedro JM, Vitale I, Aaronson SA, Abrams JM, Adam D *et al.* Essential versus accessory aspects of cell death: recommendations of the NCCD 2015. *Cell death differ* 2015; **22**: 58–73.
22 Steigemann P, Wurzenberger C, Schmitz MH, Held M, Guizetti J, Maar S *et al.* Aurora B-mediated abscission checkpoint protects against tetraploidization. *Cell* 2009; **136**: 473–484.
23 Ho LH, Read SH, Dorstyn L, Lambrusco L, Kumar S. Caspase-2 is required for cell death induced by cytoskeletal disruption. *Oncogene* 2008; **27**: 3393–3404.
24 Mhaidat NM, Wang Y, Kiejda KA, Zhang XD, Hersey P. Docetaxel-induced apoptosis in melanoma cells is dependent on activation of caspase-2. *Mol cancer therapeut* 2007; **6**: 752–761.
25 Choy H. Taxanes in combined modality therapy for solid tumors. *Crit Rev Oncol Hematol* 2001; **37**: 237–247.
26 Asteriti IA, Rensen WM, Lindon C, Lavia P, Guarguaglini G. The Aurora-A/TPX2 complex: a novel oncogenic holoenzyme? *Biochim Biophys Acta* 2010; **1806**: 230–239.
27 Gruss OJ, Wittmann M, Yokoyama H, Pepperkok R, Kufer T, Sillje H *et al.* Chromosome-induced microtubule assembly mediated by TPX2 is required for spindle formation in HeLa cells. *Nat Cell Biol* 2002; **4**: 871–879.
28 Morgan-Lappe SE, Tucker LA, Huang X, Zhang Q, Sarthy AV, Zakula D *et al.* Identification of Ras-related nuclear protein, targeting protein for xenopus kinesin-like protein 2, and stearoyl-CoA desaturase 1 as promising cancer targets from an RNAi-based screen. *Cancer res* 2007; **67**: 4390–4398.
29 Giubettini M, Asteriti IA, Scrofani J, De Luca M, Lindon C, Lavia P *et al.* Control of Aurora-A stability through interaction with TPX2. *J Cell Sci* 2011; **124**: 113–122.
30 Dutertre S, Descamps S, Prigent C. On the role of aurora-A in centrosome function. *Oncogene* 2002; **21**: 6175–6183.
31 Terasima T, Tolmach LJ. X-ray sensitivity and DNA synthesis in synchronous populations of HeLa cells. *Science* 1963; **140**: 490–492.
32 Sinclair WK, Morton RA. X-ray sensitivity during the cell generation cycle of cultured Chinese hamster cells. *Radiat Res* 1966; **29**: 450–474.
33 Panier S, Durocher D. Push back to respond better: regulatory inhibition of the DNA double-strand break response. *Nat rev Mol cell biol* 2013; **14**: 661–672.
34 Martens-de Kemp SR, Nagel R, Stigter-van Walsum M, van der Meulen IH, van Beusechem VW, Braakhuis BJ *et al.* Functional genetic screens identify genes essential for tumor cell survival in head and neck and lung cancer. *Clin cancer res* 2013; **19**: 1994–2003.
35 Xu J, Yue CF, Zhou WH, Qian YM, Zhang Y, Wang SW *et al.* Aurora-A contributes to cisplatin resistance and lymphatic metastasis in non-small cell lung cancer and predicts poor prognosis. *J Transl Med* 2014; **12**: 200.
36 Anand S, Penrhyn-Lowe S, Venkitaraman AR. AURORA-A amplification overrides the mitotic spindle assembly checkpoint, inducing resistance to Taxol. *Cancer cell* 2003; **3**: 51–62.
37 Mignogna C, Staropoli N, Botta C, De Marco C, Rizzuto A, Morelli M *et al.* Aurora Kinase A expression predicts platinum-resistance and adverse outcome in high-grade serous ovarian carcinoma patients. *J Ovarian Res* 2016; **9**: 31.
38 Hata T, Furukawa T, Sunamura M, Egawa S, Motoi F, Ohmura N *et al.* RNA interference targeting aurora kinase a suppresses tumor growth and enhances the taxane chemosensitivity in human pancreatic cancer cells. *Cancer res* 2005; **65**: 2899–2905.
39 Eyers PA, Erikson E, Chen LG, Maller JL. A novel mechanism for activation of the protein kinase Aurora A. *Curr Biol* 2003; **13**: 691–697.
40 Kufer TA, Sillje HH, Korner R, Gruss OJ, Meraldi P, Nigg EA. Human TPX2 is required for targeting Aurora-A kinase to the spindle. *J Cell Biol* 2002; **158**: 617–623.
41 Tsai MY, Wiese C, Cao K, Martin O, Donovan P, Ruderman J *et al.* A Ran signalling pathway mediated by the mitotic kinase Aurora A in spindle assembly. *Nat Cell Biol* 2003; **5**: 242–248.

42 Garrido G, Vernos I. Non-centrosomal TPX2-dependent regulation of the Aurora A kinase: functional implications for healthy and pathological cell division. *Front Oncol* 2016; **6**: 88.
43 Bian M, Fu J, Yan Y, Chen Q, Yang C, Shi Q *et al.* Short exposure to paclitaxel induces multipolar spindle formation and aneuploidy through promotion of acentrosomal pole assembly. *Sci China Life Sci* 2010; **53**: 1322–1329.
44 Scharer CD, Laycock N, Osunkoya AO, Logani S, McDonald JF, Benigno BB *et al.* Aurora kinase inhibitors synergize with paclitaxel to induce apoptosis in ovarian cancer cells. *J Transl Med* 2008; **6**: 79.
45 Mazumdar A, Henderson YC, El-Naggar AK, Sen S, Clayman GL. Aurora kinase A inhibition and paclitaxel as targeted combination therapy for head and neck squamous cell carcinoma. *Head Neck* 2009; **31**: 625–634.
46 Lin Y, Richards FM, Krippendorff BF, Bramhall JL, Harrington JA, Bapiro TE *et al.* Paclitaxel and CYC3, an aurora kinase A inhibitor, synergise in pancreatic cancer cells but not bone marrow precursor cells. *Br J Cancer* 2012; **107**: 1692–1701.
47 Sehdev V, Katsha A, Ecsedy J, Zaika A, Belkhiri A, El-Rifai W. The combination of alisertib, an investigational Aurora kinase A inhibitor, and docetaxel promotes cell death and reduces tumor growth in preclinical cell models of upper gastrointestinal adenocarcinomas. *Cancer* 2013; **119**: 904–914.
48 Manfredi MG, Ecsedy JA, Chakravarty A, Silverman L, Zhang M, Hoar KM *et al.* Characterization of Alisertib (MLN8237), an investigational small-molecule inhibitor of aurora A kinase using novel in vivo pharmacodynamic assays. *Clin cancer res* 2011; **17**: 7614–7624.
49 Zullo KM, Guo Y, Cooke L, Jirau-Serrano X, Mangone M, Scotto L *et al.* Aurora A Kinase inhibition selectively synergizes with histone deacetylase inhibitor through cytokinesis failure in T-cell lymphoma. *Clin cancer res* 2015; **21**: 4097–4109.
50 Unkel S, Belka C, Lauber K. On the analysis of clonogenic survival data: Statistical alternatives to the linear-quadratic model. *Radiat oncol* 2016; **11**: 11.
51 Kinzel L, Ernst A, Orth M, Albrecht V, Hennel R, Brix N *et al.* A novel HSP90 inhibitor with reduced hepatotoxicity synergizes with radiotherapy to induce apoptosis, abrogate clonogenic survival, and improve tumor control in models of colorectal cancer. *Oncotarget* 2016; **7**: 43199–43219.
52 Lauber K, Appel HA, Schlosser SF, Gregor M, Schulze-Osthoff K, Wesselborg S. The adapter protein apoptotic protease-activating factor-1 (Apaf-1) is proteolytically processed during apoptosis. *J Biol Chem* 2001; **276**: 29772–29781.
53 Chou TC, Talalay P. Quantitative analysis of dose-effect relationships: the combined effects of multiple drugs or enzyme inhibitors. *Adv enzyme regul* 1984; **22**: 27–55.
54 Ernst A, Anders H, Kapfhammer H, Orth M, Hennel R, Seidl K *et al.* HSP90 inhibition as a means of radiosensitizing resistant, aggressive soft tissue sarcomas. *Cancer lett* 2015; **365**: 211–222.

Supplementary Information accompanies this paper on the *Oncogene* website (http://www.nature.com/onc)